Kirchhoff migration without phases

To cite this article: Patrick Bardsley and Fernando Guevara Vasquez 2016 *Inverse Problems* **32** 105006

IOP Publishing Inverse Problems
Inverse Problems **32** (2016) 105006 (17pp) doi:10.1088/0266-5611/32/10/105006

Kirchhoff migration without phases

Patrick Bardsley[1] **and Fernando Guevara Vasquez**

Mathematics Department, University of Utah, 155 S 1400 E RM 233, Salt Lake City, UT 84112-0090, USA

E-mail: bardsley@math.utah.edu and fguevara@math.utah.edu

Received 8 January 2016, revised 20 June 2016
Accepted for publication 29 June 2016
Published 15 August 2016

Abstract

We present a simple, frequency domain, preprocessing step to Kirchhoff migration that allows the method to image scatterers when the wave field phase information is lost at the receivers, and only intensities are measured. The resulting imaging method does not require knowing the phases of the probing field or manipulating the phase of the wave field at the receivers. In a regime where the scattered field is small compared to the probing field, the problem of recovering the full-waveform scattered field from intensity data can be formulated as an embarrassingly simple least-squares problem. Although this only recovers the projection (on a known subspace) of the full-waveform scattered field, we show that, for high frequencies, this projection gives Kirchhoff images asymptotically identical to the images obtained with full waveform data. Our method can also be used when the source is modulated by a Gaussian process and autocorrelations are measured at an array of receivers.

Keywords: intensity-only imaging, correlation-based imaging, migration

(Some figures may appear in colour only in the online journal)

1. Introduction

Imaging scatterers in a homogeneous medium from full waveform data is well understood. The medium is probed with waves emanating from one or more sources and the reflections from scatterers in the medium are recorded at one or more receivers. An image of the scatterers can be formed from these recordings by using classic imaging methods such as Kirchhoff or travel time migration (see e.g. [4]); or MUSIC (see e.g. [9]). Both Kirchhoff migration and MUSIC rely on full-waveform measurements at the receivers to form an image. Here we work in the frequency domain and we assume that phase information is lost and only *intensities* can be measured at the receivers. To be more precise, if $\hat{u}_r(\omega)$ is the wave field at

[1] Author to whom any correspondence should be addressed.

receiver r and angular frequency ω, we can only measure the intensity $|\hat{u}_r(\omega)|^2$. Intensity measurements arise in a variety of physical problems, e.g. when the response time of a receiver is much larger than a typical wave period. Such is the case in optical coherence tomography [27, 28] and diffraction tomography [16, 17]. In these situations, intensities are much easier and more cost-effective to measure than full waveform data.

The setup we analyze consists of one source and N receivers, all of known location. The receivers can only record intensities and only the source intensity is known. If the scattered field is small compared to the probing field (at the receivers) then the scattered field projected onto a known subspace can be found from the intensity data by solving an underdetermined real least squares problem of size $N \times 2N$ (per frequency sample). This system is underdetermined because we are trying to use the intensity data, i.e. N real measurements, to recover the scattered field, i.e. N complex or $2N$ real numbers. Fortunately, a stationary phase argument shows that the error made by projecting the scattered field does not affect Kirchhoff imaging (for high frequencies). Moreover the least-squares problem is typically well-conditioned and its solution is embarrassingly simple: it merely costs about $2N$ complex operations (additions or multiplications). Hence our method is comparable in computational cost to Kirchhoff migration. Well-known resolution studies for Kirchhoff migration can also be used for our method.

1.1. Related work for imaging with intensities

One way of imaging with intensities is called 'phase retrieval' and consists of first recovering the phases from the intensity data and then using the reconstructed field to image. Examples of this approach include using intensity measurements at two different planes to recover full waveform measurements at a single plane [16], iterative approaches e.g. [10, 12, 18, 24] and using differential identities to relate intensity measurements with full waveform data (e.g. [19, 33]). Other methods treat intensity-only measurements as noisy measurements of full waveform data (e.g. [11]) or use optimization techniques to fit assumed models of scatterers to measured intensity data (e.g. [32]). Uniqueness for the inverse scattering from multiple frequency intensity data is guaranteed under regularity conditions on the scattering coefficient [21–23]. Also, the phase retrieval problem can be seen as the problem of recovering a vector from knowing the magnitude of its coefficients in a frame [1, 6].

The problem of imaging a few point scatterers can be reformulated as a convex optimization problem involving low rank matrices [5, 7, 34]. Alternatively the polarization identity $4\,\mathrm{Re}(\boldsymbol{u}^*\boldsymbol{v}) = \|\boldsymbol{u}+\boldsymbol{v}\|^2 - \|\boldsymbol{u}-\boldsymbol{v}\|^2$, $\boldsymbol{u}, \boldsymbol{v} \in \mathbb{C}^N$, and linear combinations of single source experiments can be used to recover dot products of two single source experiments [25]. Notice that recovering the dot product $\boldsymbol{u}^*\boldsymbol{v}$ from the polarization identity requires multiplying $\boldsymbol{u}$ and $\boldsymbol{v}$ by ± 1 or $\pm\imath$. This requires manipulation of the source phases, by e.g. introducing delays. MUSIC can then be used to image with this quadratic functional of the full waveform data [25]. Instead of directly controlling the source phases, in [2] we use two sources that send exactly the same signal from two different locations. The problem of recovering the full-waveform scattered field as measured at one receiver location is formulated as a least-squares problem, which is analyzed in [2]. The least-squares systems are typically $2N \times 2N$ and the scattered field can be recovered up to a one-dimensional nullspace that does not affect the Kirchhoff images. In contrast, the present method requires less measurements (only N), no pairwise illuminations (remark 1) and the least-squares systems are trivial to solve and (usually) well-conditioned. We show that the least squares problem can be solved by multiplying the intensity data by a phase present in the direct arrival Green's function. Chen and Huang [8] found (from a different direction) an essentially equivalent way of preprocessing the intensity data in the full-aperture case.

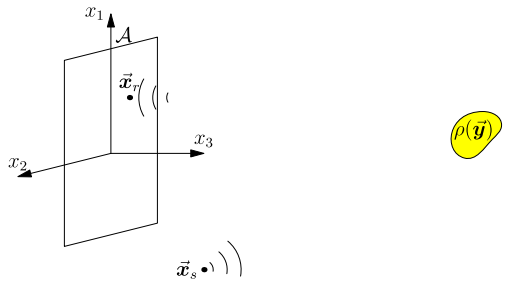

Figure 1. Physical setup for an array $\mathcal{A}$ of receivers with a wave source located at $\vec{x}_s$. The scatterer is characterized by the compactly supported function $\rho(\vec{y})$ (in yellow).

1.2. Imaging with correlations

Correlations are used for imaging when the sources are not well known. For example in seismic imaging the sources may have unknown locations [29–31] and may even consist of ambient noise [13–15]. Fortunately, the correlation of recordings at two points contains information about the Green function of the medium between the two points [13], which can be used to form an image of the medium.

As in [2] we observe that autocorrelations (i.e. correlating the recorded signal with itself) are equivalent to intensity measurements (by the Wiener–Khinchin theorem, see e.g. [20]). Therefore the method we present here can be applied to the case where only the autocorrelation (or the power spectrum) of the source is known and autocorrelations (or power spectra) are measured at the receivers. Since correlations are robust to additive noise, we expect our method to work in low signal to noise ratio situations, as we illustrate with numerical experiments.

1.3. Contents

The physical setup and notations we use are described in section 2.1 and we briefly review Kirchhoff migration in section 2.2. Using the Born approximation, we formulate the problem of recovering the full wave scattered field at the array from intensity-only measurements as a linear least squares problem section 2.3. In section 3 we analyze and solve the least squares problem and show that its solution can be used with Kirchhoff migration. We extend this imaging method to stochastic illuminations and autocorrelation measurements in section 4. Numerical experiments for an optic regime are provided in section 5 and we conclude with a discussion in section 6.

2. Wave propagation and intensity-only measurements

Here we introduce the setup we work with and briefly recall Kirchhoff migration. Hereinafter we use the Fourier transform convention for functions of time t:

$$\widehat{f}(\omega) = \int_{-\infty}^{\infty} \mathrm{d}t f(t) \mathrm{e}^{\imath\omega t}, \; f(t) = \frac{1}{2\pi} \int_{-\infty}^{\infty} \mathrm{d}\omega \widehat{f}(\omega) \mathrm{e}^{-\imath\omega t}, \quad \text{for } f(t), \; \widehat{f}(\omega) \in L^2(\mathbb{R}). \tag{1}$$

2.1. Wave propagation in a homogeneous medium

The physical setup we consider is depicted in figure 1. We probe the medium with a point source located at $\vec{\boldsymbol{x}}_s$. Waves are recorded on an array of receivers $\vec{\boldsymbol{x}}_r = (\boldsymbol{x}_r, 0) \in \mathcal{A}$ for $r = 1, \ldots, N$, where $\mathcal{A} \subset \mathbb{R}^{d-1} \times \{0\}$ and $d = 2, 3$ is the dimension. We use the notation $\boldsymbol{x}$ for the first $d - 1$ components of a vector $\vec{\boldsymbol{x}} \in \mathbb{R}^d$. For simplicity we consider a linear array in 2D or a square array in 3D, i.e. $\mathcal{A} = [-a/2, a/2]^{d-1} \times \{0\}$, however other shapes may be considered. We impose only mild conditions on the positions of the source and receivers, in particular that the source is not in the array. We assume the medium contains scatterers with reflectivity $\rho(\vec{\boldsymbol{y}})$ with $\text{supp}(\rho) = \mathcal{R}$, and background wave velocity c_0.

The total field arriving at the receiver location $\vec{\boldsymbol{x}}_r$ from frequency modulation $\widehat{f}(\omega)$ at the source location $\vec{\boldsymbol{x}}_s$ is

$$\hat{u}(\vec{\boldsymbol{x}}_r, \vec{\boldsymbol{x}}_s, \omega) = \widehat{G}(\vec{\boldsymbol{x}}_r, \vec{\boldsymbol{x}}_s, \omega)\widehat{f}(\omega), \tag{2}$$

where $\widehat{G}$ is the Green's function for the (inhomogeneous) medium in the frequency domain. We assume the scatterers are weak so that multiple scatterings may be neglected and by the Born approximation

$$\widehat{G}(\vec{\boldsymbol{x}}_r, \vec{\boldsymbol{x}}_s, \omega) \approx \widehat{G}_0(\vec{\boldsymbol{x}}_r, \vec{\boldsymbol{x}}_s, \omega) + k^2 \int_{\mathcal{R}} \mathrm{d}\vec{\boldsymbol{y}}\, \rho(\vec{\boldsymbol{y}}) \widehat{G}_0(\vec{\boldsymbol{x}}_r, \vec{\boldsymbol{y}}, \omega) \widehat{G}_0(\vec{\boldsymbol{y}}, \vec{\boldsymbol{x}}_s, \omega), \tag{3}$$

where $\widehat{G}_0$ is the Green's function for the Helmholtz equation:

$$\widehat{G}_0(\vec{\boldsymbol{x}}, \vec{\boldsymbol{y}}, \omega) = \begin{cases} \frac{\imath}{4} H_0^{(1)}(k|\vec{\boldsymbol{x}} - \vec{\boldsymbol{y}}|), & d = 2, \\ \frac{\exp(\imath k |\vec{\boldsymbol{x}} - \vec{\boldsymbol{y}}|)}{4\pi |\vec{\boldsymbol{x}} - \vec{\boldsymbol{y}}|}, & d = 3. \end{cases} \tag{4}$$

Here $k = \omega/c_0$ is the wave number.

We express the total fields received on the array with linear algebra notation as

$$u(\vec{\boldsymbol{x}}_r, \vec{\boldsymbol{x}}_s, \omega) = \boldsymbol{e}_r^{\mathsf{T}} (\boldsymbol{g}_0(\vec{\boldsymbol{x}}_s, \omega) + \boldsymbol{p}(\vec{\boldsymbol{x}}_s, \omega))\widehat{f}(\omega), \quad \text{for } r = 1, \ldots, N,$$

where $\{\boldsymbol{e}_r\}_{r=1}^N$ is the standard orthonormal basis of $\mathbb{R}^N$, the vector $\boldsymbol{g}_0$ is the vector of direct arrivals (or incident field) at the array

$$\boldsymbol{g}_0(\vec{\boldsymbol{x}}_s, \omega) = [\widehat{G}_0(\vec{\boldsymbol{x}}_1, \vec{\boldsymbol{x}}_s, \omega), \widehat{G}_0(\vec{\boldsymbol{x}}_2, \vec{\boldsymbol{x}}_s, \omega), \ldots, \widehat{G}_0(\vec{\boldsymbol{x}}_N, \vec{\boldsymbol{x}}_s, \omega)]^{\mathsf{T}} \tag{5}$$

and the array response vector (or scattered field at the array) is

$$\boldsymbol{p}(\vec{\boldsymbol{x}}_s, \omega) = k^2 \int_{\mathcal{R}} \mathrm{d}\vec{\boldsymbol{z}}\, \boldsymbol{g}_0(\vec{\boldsymbol{z}}, \omega) \widehat{G}_0(\vec{\boldsymbol{x}}_s, \vec{\boldsymbol{z}}, \omega) \rho(\vec{\boldsymbol{z}}). \tag{6}$$

2.2. Kirchhoff migration

When full waveform measurements are available, i.e. $u(\vec{\boldsymbol{x}}_r, \vec{\boldsymbol{x}}_s, \omega)$ is known for $r = 1, \ldots, N$, the scattered field $\boldsymbol{p}$ can be obtained from the total field at the array, $\boldsymbol{g}_0$ and $\widehat{f}(\omega)$. The scatterers in the medium can be imaged with Kirchhoff migration applied to $\boldsymbol{p}$, which for a single frequency ω has the form:

$$\Gamma_{\text{KM}}[\boldsymbol{p}, \omega](\vec{\boldsymbol{y}}) = \overline{\widehat{G}_0}(\vec{\boldsymbol{x}}_s, \vec{\boldsymbol{y}}, \omega) \boldsymbol{g}_0(\vec{\boldsymbol{y}}, \omega)^* \boldsymbol{p}(\vec{\boldsymbol{x}}_s, \omega). \tag{7}$$

Here $\vec{\boldsymbol{y}}$ is a point in the image and $\boldsymbol{a}^*$ denotes the Hermitian transpose of a vector $\boldsymbol{a}$. The Kirchhoff migration functional has been studied extensively (see e.g. Bleistein *et al* [4] for a review). In the cross-range (the direction parallel to the array), we can expect a resolution of $\lambda L/a$, where $\lambda = 2\pi/k$ is the wavelength, L is the array to scatterer distance and a is array

aperture. This is the Rayleigh resolution limit. To obtain resolution in the range direction (the direction perpendicular to the array), $\Gamma_{\mathrm{KM}}[\boldsymbol{p}, \omega]$ needs to be integrated over a frequency band $\mathcal{B}$, e.g. $\mathcal{B} = [-\omega_{\max}, -\omega_{\min}] \cup [\omega_{\min}, \omega_{\max}]$. In this case we can expect the resolution to be $c_0/(\omega_{\max} - \omega_{\min})$.

2.3. Intensity-only measurements

Using the illumination $\widehat{f}(\omega)$ at the source location $\vec{\boldsymbol{x}}_s$, the *intensity-only* measurement of the wave field at $\vec{\boldsymbol{x}}_r \in \mathcal{A}$ is:

$$|u(\vec{\boldsymbol{x}}_r, \vec{\boldsymbol{x}}_s, \omega)|^2 = |\widehat{f}(\omega)|^2 \boldsymbol{e}_r^{\mathsf{T}} [\overline{(\boldsymbol{g}_0 + \boldsymbol{p})} \odot (\boldsymbol{g}_0 + \boldsymbol{p})], \tag{8}$$

where the operator $\odot$ denotes the componentwise or Hadamard product of two vectors. Our objective is to find as much as we can about $\boldsymbol{p}$ from the vector of measurements $[|u(\vec{\boldsymbol{x}}_r, \vec{\boldsymbol{x}}_s, \omega)|^2]_{r=1,\ldots,N}$. This is done by linearization, so we need to assume that the scattered field $\boldsymbol{p}$ is small compared to the direct arrival $\boldsymbol{g}_0$ at the array.

Assumption 1. The position of the receivers, the source and the reflectivity are such that $|\boldsymbol{e}_r^{\mathsf{T}} \boldsymbol{p}| \ll |\boldsymbol{e}_r^{\mathsf{T}} \boldsymbol{g}_0|$, $r = 1, \ldots, N$.

This assumption is satisfied e.g. if the reflectivity is sufficiently small and the source $\vec{\boldsymbol{x}}_s$ is near the receiver array (as is shown in figure 1). With assumption 1 we can neglect quadratic terms in $\boldsymbol{p}$ to approximate the intensity measurements (8) by a vector $\boldsymbol{d}(\vec{\boldsymbol{x}}_s, \omega)$ defined by

$$|u(\vec{\boldsymbol{x}}_r, \vec{\boldsymbol{x}}_s, \omega)|^2 \approx \boldsymbol{e}_r^{\mathsf{T}} \boldsymbol{d}(\vec{\boldsymbol{x}}_s, \omega) \equiv |\widehat{f}(\omega)|^2 \boldsymbol{e}_r^{\mathsf{T}} \operatorname{Re}[\overline{\boldsymbol{g}}_0 \odot (\boldsymbol{g}_0 + 2\boldsymbol{p})].$$

This is not, strictly speaking, a linear system for $\boldsymbol{p} \in \mathbb{C}^N$ since $\boldsymbol{u} \to \operatorname{Re}(\boldsymbol{u})$ is not a linear mapping from $\mathbb{C}^N$ to $\mathbb{C}^N$. However we can write an underdetermined linear system for the real and imaginary parts of $\boldsymbol{g}_0 + 2\boldsymbol{p}$ as follows

$$|\widehat{f}(\omega)|^2 \mathsf{M}(\vec{\boldsymbol{x}}_s, \omega) \begin{bmatrix} \operatorname{Re}(\boldsymbol{g}_0 + 2\boldsymbol{p}) \\ \operatorname{Im}(\boldsymbol{g}_0 + 2\boldsymbol{p}) \end{bmatrix} = \boldsymbol{d}(\vec{\boldsymbol{x}}_s, \omega), \tag{9}$$

where the matrix $\mathsf{M}(\vec{\boldsymbol{x}}_s, \omega) \in \mathbb{R}^{N \times 2N}$ is given by

$$\mathsf{M}(\vec{\boldsymbol{x}}_s, \omega) = \begin{bmatrix} \mathsf{diag}(\operatorname{Re}(\boldsymbol{g}_0)) & \mathsf{diag}(\operatorname{Im}(\boldsymbol{g}_0)) \end{bmatrix}. \tag{10}$$

We give in the next section an explicit solution to the least squares problem (9).

3. Migrating a least-squares estimate of the scattered field

The first step in our imaging method consists of a cheap least-squares preprocessing step that gives an approximation to the array response vector (section 3.1). The second step is to migrate this approximation with standard Kirchhoff migration section 3.2. Crucially we show in theorem 1 that the mistake we make by using this approximation of the array response vector does not affect the Kirchhoff images.

3.1. Recovering a projection of the array response vector

We start by finding a simple and explicit expression to the pseudoinverse of the matrix M that we obtained from linearizing the problem of finding the real and imaginary parts of the array response vector $\boldsymbol{p}$. This can be used to recover from the data $\boldsymbol{d}$ the orthogonal projection of

$[\,\mathrm{Re}(\boldsymbol{p})^{\mathsf{T}}, \mathrm{Im}(\boldsymbol{p})^{\mathsf{T}}]^{\mathsf{T}}$ onto a known N-dimensional subspace (that depends only on $\boldsymbol{g}_0$). Moreover the process is well conditioned.

First notice that the matrix M is full-rank. Indeed a simple calculation gives that $\mathsf{M}\overline{\mathsf{M}}^{\mathsf{T}} = \mathsf{diag}(\overline{\boldsymbol{g}}_0 \odot \boldsymbol{g}_0)$. This matrix is clearly invertible because it is a diagonal matrix with the moduli of 2D or 3D Green functions on the diagonal. Hence the Moore–Penrose pseudoinverse $\mathsf{M}^{\dagger}$ can be written explicitly

$$\mathsf{M}^{\dagger} = \mathsf{M}^{\mathsf{T}}(\mathsf{M}\overline{\mathsf{M}}^{\mathsf{T}})^{-1} = \begin{bmatrix} \mathsf{diag}(\,\mathrm{Re}(\boldsymbol{g}_0)) \\ \mathsf{diag}(\,\mathrm{Im}(\boldsymbol{g}_0)) \end{bmatrix} \mathsf{diag}(\overline{\boldsymbol{g}}_0 \odot \boldsymbol{g}_0)^{-1}. \tag{11}$$

We can use $\mathsf{M}^{\dagger}$ to see what information about $\boldsymbol{p}$ we can recover from the right-hand side $\boldsymbol{d}$ in the least-squares problem (9). Since M has an N-dimensional nullspace, we can only expect to recover the orthogonal projection of $[\,\mathrm{Re}(\boldsymbol{p})^{\mathsf{T}}, \mathrm{Im}(\boldsymbol{p})^{\mathsf{T}}]^{\mathsf{T}}$ onto $\mathrm{range}(\overline{\mathsf{M}}^{\mathsf{T}}) = (\mathrm{null}(\mathsf{M}))^{\perp}$. This projection has a simple form when we write it in $\mathbb{C}^N$, as can be seen in the next proposition.

Proposition 1. *Provided $|\widehat{f}\,(\omega)|^2 \neq 0$, the intensity measurements $\boldsymbol{d}$ determine*

$$\widetilde{\boldsymbol{p}} \equiv \boldsymbol{p} + (\overline{\boldsymbol{g}}_0)^{-1} \odot \boldsymbol{g}_0 \odot \overline{\boldsymbol{p}}\,, \tag{12}$$

where the inverse of a vector is understood componentwise. Moreover $\widetilde{\boldsymbol{p}}$ can be obtained in about $2N$ complex operations from $\boldsymbol{d}$ with

$$\widetilde{\boldsymbol{p}} = |\widehat{f}\,(\omega)|^{-2}(\overline{\boldsymbol{g}}_0)^{-1} \odot \boldsymbol{d} - \boldsymbol{g}_0. \tag{13}$$

Proof. Since we use the first (resp. last) N rows of $\mathsf{M}^{\dagger}$ to recover the real (resp. imaginary) part of a vector in $\mathbb{C}^N$, it is convenient to consider the matrix

$$[\mathsf{I} \;\; i\mathsf{I}]\mathsf{M}^{\dagger} = \mathsf{diag}(\boldsymbol{g}_0)\mathsf{diag}(\overline{\boldsymbol{g}}_0 \odot \boldsymbol{g}_0)^{-1} = \mathsf{diag}(\overline{\boldsymbol{g}}_0)^{-1},$$

where I is the $N \times N$ identity matrix. To see what information about $\boldsymbol{p}$ we can recover from the right-hand side $\boldsymbol{d}$ in the least-squares system (9) we can evaluate:

$$\begin{aligned} |\widehat{f}\,(\omega)|^{-2}[\mathsf{I} \;\; i\mathsf{I}]\mathsf{M}^{\dagger}\boldsymbol{d} &= \mathsf{diag}(\overline{\boldsymbol{g}}_0)^{-1}\mathsf{M}\begin{bmatrix} \mathrm{Re}\,(\boldsymbol{g}_0 + 2\boldsymbol{p}) \\ \mathrm{Im}(\boldsymbol{g}_0 + 2\boldsymbol{p}) \end{bmatrix} \\ &= \mathsf{diag}(\overline{\boldsymbol{g}}_0)^{-1}[\,\mathrm{Re}\,(\boldsymbol{g}_0)^2 + \mathrm{Im}\,(\boldsymbol{g}_0)^2 + 2\,\mathrm{Re}\,(\boldsymbol{g}_0)\,\mathrm{Re}\,(\boldsymbol{p}) + 2\,\mathrm{Im}\,(\boldsymbol{g}_0)\,\mathrm{Im}\,(\boldsymbol{p})] \\ &= \boldsymbol{g}_0 + \mathsf{diag}(\overline{\boldsymbol{g}}_0)^{-1}(\boldsymbol{g}_0 \odot \overline{\boldsymbol{p}} + \overline{\boldsymbol{g}}_0 \odot \boldsymbol{p}) \\ &= \boldsymbol{g}_0 + \boldsymbol{p} + \boldsymbol{g}_0 \odot (\overline{\boldsymbol{g}}_0)^{-1} \odot \overline{\boldsymbol{p}} = \boldsymbol{g}_0 + \widetilde{\boldsymbol{p}}\,. \end{aligned}$$

Hence we can get $\widetilde{\boldsymbol{p}}$ from the intensity data $\boldsymbol{d}$ with essentially N complex multiplications and N complex additions. □

A natural question to ask is whether we can obtain $\widetilde{\boldsymbol{p}}$ in a stable manner from $\boldsymbol{d}$. This can be answered by looking at the conditioning of M, i.e. the ratio of the largest singular value σ_1 of M to σ_N, the smallest one. These are easily obtained from the square roots of the eigenvalues of the diagonal matrix $\mathsf{M}\overline{\mathsf{M}}^{\mathrm{T}} = \mathsf{diag}(\overline{\boldsymbol{g}}_0 \odot \boldsymbol{g}_0)$. Hence the conditioning of M is the ratio of the largest to the smallest moduli of the entries of $\boldsymbol{g}_0$:

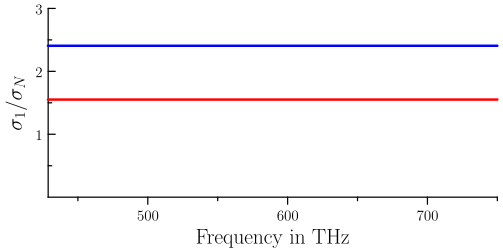

Figure 2. Condition number of $\mathsf{M}(\vec{\boldsymbol{x}}_s, \omega)$ for $d = 2$ (red) and $d = 3$ (blue) for the setup given in section 5.

$$\text{cond}(\mathsf{M}) = \begin{cases} \dfrac{\max_r |H_0^{(1)}(k|\vec{\boldsymbol{x}}_r - \vec{\boldsymbol{x}}_s|)|}{\min_r |H_0^{(1)}(k|\vec{\boldsymbol{x}}_r - \vec{\boldsymbol{x}}_s|)|}, & \text{for } d = 2, \\ \dfrac{\max_r|\vec{\boldsymbol{x}}_r - \vec{\boldsymbol{x}}_s|}{\min_r|\vec{\boldsymbol{x}}_r - \vec{\boldsymbol{x}}_s|}, & \text{for } d = 3. \end{cases} \tag{14}$$

In figure 2 we show the condition number of $\mathsf{M}(\vec{\boldsymbol{x}}_s, \omega)$ plotted over an optical frequency band. The experimental setup is that given in section 5. The condition number (14) is clearly independent of frequency for $d = 3$ and for $d = 2$ we have the approximation for high frequencies:

$$\text{cond}\,\mathsf{M}(\vec{\boldsymbol{x}}_s, \omega) = \frac{\max_r\ |\vec{\boldsymbol{x}}_r - \vec{\boldsymbol{x}}_s|^{1/2}}{\min_r\ |\vec{\boldsymbol{x}}_r - \vec{\boldsymbol{x}}_s|^{1/2}}(1 + O(1/\omega)), \quad \text{as } \omega \to \infty.$$

This approximation follows from the Hankel function asymptotic (see e.g. [26])

$$H_0^{(1)}(t) = \sqrt{\frac{2}{\pi t}}\,\exp[\imath(t - \pi/4)](1 + \mathcal{O}(1/t)), \quad \text{as } t \to \infty.$$

Thus the conditioning of M is determined by the ratio of largest to smallest source-to-receiver distances.

3.2. Kirchhoff migration

We now show that migrating the recovered data $\tilde{\boldsymbol{p}}$ (12) using Γ_{KM} gives essentially the same image as migrating the true data $\boldsymbol{p}$. We establish this result by means of a stationary phase argument but in order to do this, we need the following assumption on the location of the source $\vec{\boldsymbol{x}}_s$.

Assumption 2 (**Geometric imaging conditions**). For a scattering potential with support contained inside an image window $\mathcal{W}$, we assume $\vec{\boldsymbol{x}}_s$ satisfies

$$\frac{\vec{\boldsymbol{x}}_r - \vec{\boldsymbol{x}}_s}{|\vec{\boldsymbol{x}}_r - \vec{\boldsymbol{x}}_s|} \neq \frac{\vec{\boldsymbol{x}}_r - \vec{\boldsymbol{y}}}{|\vec{\boldsymbol{x}}_r - \vec{\boldsymbol{y}}|},$$

for $r = 1, \ldots, N$, and $\vec{\boldsymbol{y}} \in \mathcal{W}$.

We interpret this assumption as a restriction on the placement of our source location $\vec{\boldsymbol{x}}_s$ as follows. Fix a receiver position $\vec{\boldsymbol{x}}_r$ and consider the cone

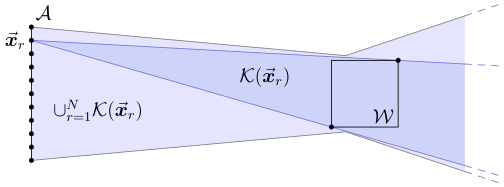

Figure 3. Illustration of assumption 2. If $\vec{x}_s$ is outside of the light blue region then $(\vec{x}_r - \vec{x}_s)/|\vec{x}_r - \vec{x}_s| \neq (\vec{x}_r - \vec{y})/|\vec{x}_r - \vec{y}|$ for all $\vec{x}_r \in \mathcal{A}$ and $\vec{y} \in \mathcal{W}$.

$$\mathcal{K}(\vec{x}_r) = \left\{ \alpha \frac{\vec{y} - \vec{x}_r}{|\vec{y} - \vec{x}_r|} : \alpha > 0, \vec{y} \in \mathcal{W} \right\}.$$

As long as $\vec{x}_s \notin \mathcal{K}(\vec{x}_r)$, then we have that $(\vec{x}_s - \vec{x}_r)/|\vec{x}_s - \vec{x}_r| \neq (\vec{y} - \vec{x}_r)/|\vec{y} - \vec{x}_r|$ for any $\vec{y} \in \mathcal{W}$, i.e. assumption 2 holds for $\vec{x}_r$. Ensuring this is satisfied for all receiver locations $\vec{x}_r$ for $r = 1,\ldots,N$, we require $\vec{x}_s \notin \cup_{r=1}^N \mathcal{K}(\vec{x}_r)$. In figure 3 we illustrate this assumption. Here, the dark blue region depicts the cone $\mathcal{K}(\vec{x}_r)$ while the union of cones $\cup_{r=1}^N \mathcal{K}(\vec{x}_r)$ is depicted by the light blue region. Assumption 2 simply requires $\vec{x}_s$ to be outside the light blue region.

Theorem 1. *Provided assumption 2 holds, the image of the reconstructed array response vector is*

$$\Gamma_{\mathrm{KM}}[\boldsymbol{p} + (\overline{\boldsymbol{g}}_0)^{-1} \odot \boldsymbol{g}_0 \odot \overline{\boldsymbol{p}}\,, \omega](\vec{\boldsymbol{y}}) \approx \Gamma_{\mathrm{KM}}[\boldsymbol{p}, \omega](\vec{\boldsymbol{y}}).$$

Proof. We begin by approximating the Kirchhoff migration functional (7) by an integral over the array $\mathcal{A}$:

$$\begin{aligned}
&\Gamma_{\mathrm{KM}}[(\overline{\boldsymbol{g}}_0)^{-1} \odot \boldsymbol{g}_0 \odot \overline{\boldsymbol{p}}\,](\vec{\boldsymbol{y}}) \\
&\quad = \overline{\widehat{G}_0}(\vec{x}_s, \vec{y}\,, \omega)\boldsymbol{g}_0(\vec{\boldsymbol{y}}, \omega)^*[(\overline{\boldsymbol{g}}_0(\vec{\boldsymbol{x}}_s, \omega))^{-1} \odot \boldsymbol{g}_0(\vec{\boldsymbol{x}}_s, \omega) \odot \overline{\boldsymbol{p}}\,(\vec{\boldsymbol{x}}_s, \omega)] \\
&\quad \sim k^2 \int_{\mathcal{R}} \mathrm{d}\vec{z} \int_{\mathcal{A}} \mathrm{d}\boldsymbol{x}_r\, C(\vec{x}_s, \vec{x}_r, \vec{z}\,, \vec{y}\,) \times \exp(\imath k(2|\vec{x}_r - \vec{x}_s| - |\vec{x}_r - \vec{z}| \\
&\qquad - |\vec{z} - \vec{x}_s| - |\vec{x}_r - \vec{y}\,| - |\vec{y} - \vec{x}_s|)).
\end{aligned} \tag{15}$$

Here $\sim$ denotes equal up to a constant and $C(\vec{x}_s, \vec{x}_r, \vec{z}\,, \vec{y}\,)$ is a smooth real valued function that collects the various $\widehat{G}_0$ geometric spreading terms.

Now we apply the method of stationary phase (see e.g. [4]) to the integral over $\mathcal{A}$. In the large wavenumber limit $k \to \infty$, dominant contributions to the integral come from stationary points of the phase, i.e. points $\vec{x}_r$ that satisfy

$$\nabla_{\vec{x}_r}(2|\vec{x}_r - \vec{x}_s| - |\vec{x}_r - \vec{z}| - |\vec{z} - \vec{x}_s| - |\vec{x}_r - \vec{y}\,| - |\vec{y} - \vec{x}_s|) = 0.$$

This expression is equivalent to

$$\frac{\vec{x}_r - \vec{x}_s}{|\vec{x}_r - \vec{x}_s|} = \frac{1}{2}\left(\frac{\vec{x}_r - \vec{y}}{|\vec{x}_r - \vec{y}\,|} + \frac{\vec{x}_r - \vec{z}}{|\vec{x}_r - \vec{z}|} \right). \tag{16}$$

If (16) holds then we must have

$$\left| \frac{\vec{x}_r - \vec{x}_s}{|\vec{x}_r - \vec{x}_s|} \right|^2 = \frac{1}{4} \left| \frac{\vec{x}_r - \vec{y}}{|\vec{x}_r - \vec{y}|} + \frac{\vec{x}_r - \vec{z}}{|\vec{x}_r - \vec{z}|} \right|^2$$
$$\iff 1 = \frac{\vec{x}_r - \vec{y}}{|\vec{x}_r - \vec{y}|} \cdot \frac{\vec{x}_r - \vec{z}}{|\vec{x}_r - \vec{z}|}. \tag{17}$$

Since $(\vec{x}_r - \vec{y})/|\vec{x}_r - \vec{y}|$ and $(\vec{x}_r - \vec{z})/|\vec{x}_r - \vec{z}|$ are both unit vectors, it follows from the Cauchy–Schwarz *equality* that (17) holds only if $\vec{z} = \vec{y}$. Thus stationary points must satisfy

$$\frac{\vec{x}_r - \vec{x}_s}{|\vec{x}_r - \vec{x}_s|} = \frac{\vec{x}_r - \vec{y}}{|\vec{x}_r - \vec{y}|},$$

where $\vec{y} \in \mathcal{W}$. By assumption 2 there are no such stationary points and therefore, neglecting boundary effects, this integral vanishes faster than any polynomial power of ω (see e.g. [3]). □

Remark 1. We used a similar idea in [2] to show that with multiple sources, a single receiver, and a specific pairwise illumination scheme it is possible to image with sole knowledge of the intensities of the wave fields at the receiver and of the probing fields. We approached the problem by estimating the array response vector (a vector in $\mathbb{C}^N$) with $2N$ (or more) real measurements, which are essentially the measured intensities for $2N$ or more different pairs of sources. The results of sections 3.1 and 3.2 can be modified by reciprocity to apply to the setup we considered in [2]. Hence images similar to those in [2] can be obtained without the pairwise illumination scheme and the number of required illuminations is reduced from $3N$ to N.

4. Stochastic illuminations and autocorrelations

Our imaging method can also be used when the source is driven by a stationary stochastic process (for which we only assume knowledge of the autocorrelation or power spectra) and only empirical autocorrelations are measured at the receiver locations.

To be more precise, the source at $\vec{x}_s$ is driven by $f(t)$, a stationary mean zero Gaussian process with autocorrelation function

$$\langle \overline{f}(t) f(t+\tau) \rangle = F(\tau). \tag{18}$$

Here $\langle \cdot \rangle$ denotes expectation with respect to realizations of f and we recall that $F(\tau) = \overline{F}(-\tau)$. In the time domain, the field recorded at $\vec{x}_r$ is

$$u(\vec{x}_r, \vec{x}_s, t) = \frac{1}{2\pi} \int \mathrm{d}\omega \mathrm{e}^{-\imath\omega t} \widehat{G}(\vec{x}_r, \vec{x}_s, \omega) \widehat{f}(\omega), \qquad \text{for } r = 1, \ldots, N,$$

where we assume $\widehat{G}$ is given by the Born approximation (3).

The measurements at the receiver locations $\vec{x}_r$ are the empirical autocorrelations:

$$\psi(\vec{x}_r, \vec{x}_s, \tau) = \frac{1}{2T} \int_{-T}^{T} \mathrm{d}t \overline{u}(\vec{x}_r, \vec{x}_s, t) u(\vec{x}_r, \vec{x}_s, t+\tau) \qquad \text{for } r = 1, \ldots, N, \tag{19}$$

where T is a fixed acquisition time. As shown by Garnier and Papanicolaou [13], these measurements are independent of the acquisition time T and ergodic as we summarize in the following proposition.

Proposition 2. *Assume $f(t)$ is a stationary mean zero Gaussian process satisfying (18). The expectation of the empirical autocorrelations (19) is independent of the acquisition time T:*

$$\langle \psi(\vec{\boldsymbol{x}}_r, \vec{\boldsymbol{x}}_s, \tau) \rangle = \Psi(\vec{\boldsymbol{x}}_r, \vec{\boldsymbol{x}}_s, \tau),$$

where

$$\Psi(\vec{\boldsymbol{x}}_r, \vec{\boldsymbol{x}}_s, \tau) = \frac{1}{2\pi} \int \mathrm{d}\omega \mathrm{e}^{-\imath\omega\tau} \widehat{F}(\omega) \boldsymbol{e}_r^{\mathsf{T}} [\overline{\boldsymbol{g}}(\vec{\boldsymbol{x}}_s, \omega) \odot \boldsymbol{g}(\vec{\boldsymbol{x}}_s, \omega)], \tag{20}$$

with $\boldsymbol{g} \equiv \boldsymbol{g}_0 + \boldsymbol{p}$. Furthermore, (19) is ergodic, i.e.

$$\psi(\vec{\boldsymbol{x}}_r, \vec{\boldsymbol{x}}_s, \tau) \overset{T\to\infty}{\longrightarrow} \Psi(\vec{\boldsymbol{x}}_r, \vec{\boldsymbol{x}}_s, \tau). \tag{21}$$

Proof. The proof is a straight-forward application of [13, proposition 4.1]. □

The ergodicity (21) of this proposition guarantees that for sufficiently large acquisition time T, the autocorrelation $\psi(\vec{\boldsymbol{x}}_r, \vec{\boldsymbol{x}}_s, \tau)$ is close to an intensity measurement, i.e.

$$\widehat{\psi}(\vec{\boldsymbol{x}}_r, \vec{\boldsymbol{x}}_s, \omega) \overset{T\to\infty}{\longrightarrow} \widehat{\Psi}(\vec{\boldsymbol{x}}_r, \vec{\boldsymbol{x}}_s, \omega) = \widehat{F}(\omega) \boldsymbol{e}_r^{\mathsf{T}} [\overline{(\boldsymbol{g}_0 + \boldsymbol{p})} \odot (\boldsymbol{g}_0 + \boldsymbol{p})].$$

Proceeding analogously as in section 2.3, we neglect the quadratic term in $\boldsymbol{p}$:

$$\widehat{\Psi}(\vec{\boldsymbol{x}}_r, \vec{\boldsymbol{x}}_s, \omega) \approx \widehat{F}(\omega) \boldsymbol{e}_r^{\mathsf{T}} \operatorname{Re}(\overline{\boldsymbol{g}}_0 \odot (\boldsymbol{g}_0 + 2\boldsymbol{p})).$$

The collection of autocorrelations for $r = 1, \ldots, N$ can be expressed, approximately, as

$$[\widehat{\Psi}(\vec{\boldsymbol{x}}_r, \vec{\boldsymbol{x}}_s, \omega)]_{r=1,\ldots,N} \approx \boldsymbol{d}(\vec{\boldsymbol{x}}_s, \omega) \equiv \widehat{F}(\omega) \mathsf{M}(\vec{\boldsymbol{x}}_s, \omega) \begin{bmatrix} \operatorname{Re}(\boldsymbol{g}_0 + 2\boldsymbol{p}) \\ \operatorname{Im}(\boldsymbol{g}_0 + 2\boldsymbol{p}) \end{bmatrix},$$

where $\mathsf{M}(\vec{\boldsymbol{x}}_s, \omega) \in \mathbb{R}^{N\times 2N}$ is given by (10). Therefore, the techniques developed in section 3 can be applied to image from the autocorrelation measurements (19).

5. Numerical experiments

We now provide 2D numerical experiments of our proposed imaging method. The physical scalings we use correspond to an optic regime. We use the background wave velocity of $c_0 = 3 \times 10^8$ m s^{-1} and central frequency of about 590 THz which gives a central wavelength λ_0 of about 509 nm. Our receiver array $\mathcal{A}$ is a linear array centered at the origin and consists of 501 receivers located at coordinates $\vec{\boldsymbol{x}}_r = (0, -5 + (r-1)(10/500))$ mm for $r = 1, \ldots, 501$. This corresponds to using a 1 cm linear array of receivers spaced approximately 20 μm apart. We place the wave source at coordinate $\vec{\boldsymbol{x}}_s = (5, -7.5)$ mm to guarantee assumption 2 is satisfied. We begin with experiments in the deterministic setting (section 5.1) followed by an experiment in the stochastic setting (section 5.2). Lastly, we investigate situations where assumptions 1 and/or 2 are violated and our method is not expected to work (section 5.3). For all experiments, we assume 3D wave propagation for simplicity so that $\widehat{G}_0$ is given by (4) for $d = 3$.

5.1. Deterministic illuminations

Using the illumination $\widehat{f}(\omega) \equiv 1$, we generate the intensity data $\boldsymbol{d}(\vec{\boldsymbol{x}}_s, \omega)$ using the Born approximation:

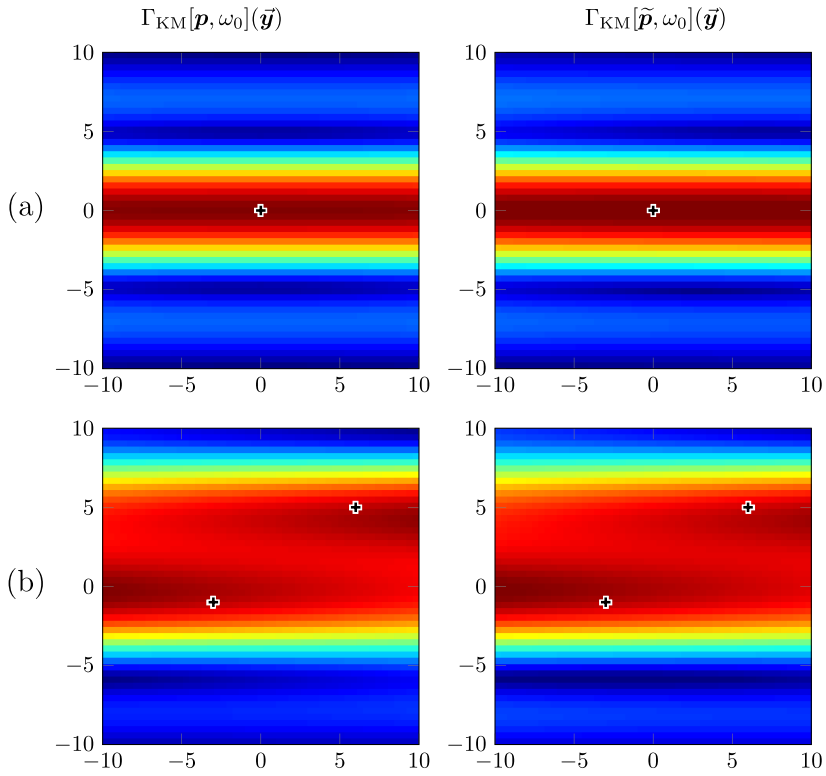

Figure 4. Single frequency Kirchhoff images of (a) one and (b) two point scatterers whose true locations are indicated by crosses. The left column uses the full array response vector $\boldsymbol{p}$ while the right column uses the array response vector $\widetilde{\boldsymbol{p}}$ recovered from intensity data. The horizontal and vertical axes display the range and cross-range respectively, measured in central wavelengths λ_0 from (50, 0) mm. The images are generated for the central frequency $(2\pi)^{-1}\omega_0 = 590$ THz.

$$\boldsymbol{d}\,(\vec{\boldsymbol{x}}_s,\,\omega) = \overline{(\boldsymbol{g}_0 + \boldsymbol{p})} \odot (\boldsymbol{g}_0 + \boldsymbol{p}),$$

with $\boldsymbol{g}_0$ and $\boldsymbol{p}$ defined by (5) and (6) respectively, for 100 uniformly spaced frequencies in the frequency band [430, 750] THz. This corresponds to obtaining intensity data for 100 different monochromatic illuminations with wavelengths $\lambda \in [400, 700]$ nm, equally spaced in the frequency band. Note that the quadratic term $\overline{\boldsymbol{p}} \odot \boldsymbol{p}$ is present in our data, but using assumption 1 we proceed assuming $\boldsymbol{d}$ is well approximated by the linear system (9).

We recover the approximate array response vector $\widetilde{\boldsymbol{p}} = (\overline{\boldsymbol{g}}_0)^{-1} \odot \boldsymbol{d} - \boldsymbol{g}_0$ for each frequency ω in the angular frequency band $\mathcal{B}$, where $(2\pi)^{-1}\mathcal{B} = [430, 750]$ THz. An image is then formed using the Kirchhoff migration functional integrated over $\mathcal{B}$:

$$\Gamma_{\mathrm{KM}}[\widetilde{\boldsymbol{p}}](\vec{\boldsymbol{y}}) = \int_{\mathcal{B}} \mathrm{d}\omega \Gamma_{\mathrm{KM}}[\widetilde{\boldsymbol{p}},\,\omega](\vec{\boldsymbol{y}}),$$

where Γ_{KM} is defined in (7). Here we consider image points $\vec{\boldsymbol{y}} \in \mathcal{W} = \{(50\text{ mm} + i\lambda_0/2.5, j\lambda_0/2.5), \text{for } i, j = -25, \ldots, 25\}$.

For our first experiment, we consider a point reflector located at coordinate $\vec{\boldsymbol{y}} = (50, 0)$ mm with refractive index perturbation $\rho(\vec{\boldsymbol{y}}) = 1 \times 10^{-15}$ (roughly equivalent to a reflector of area $(\lambda_0)^2$ and reflectivity 5978). We present the Kirchhoff image at the central

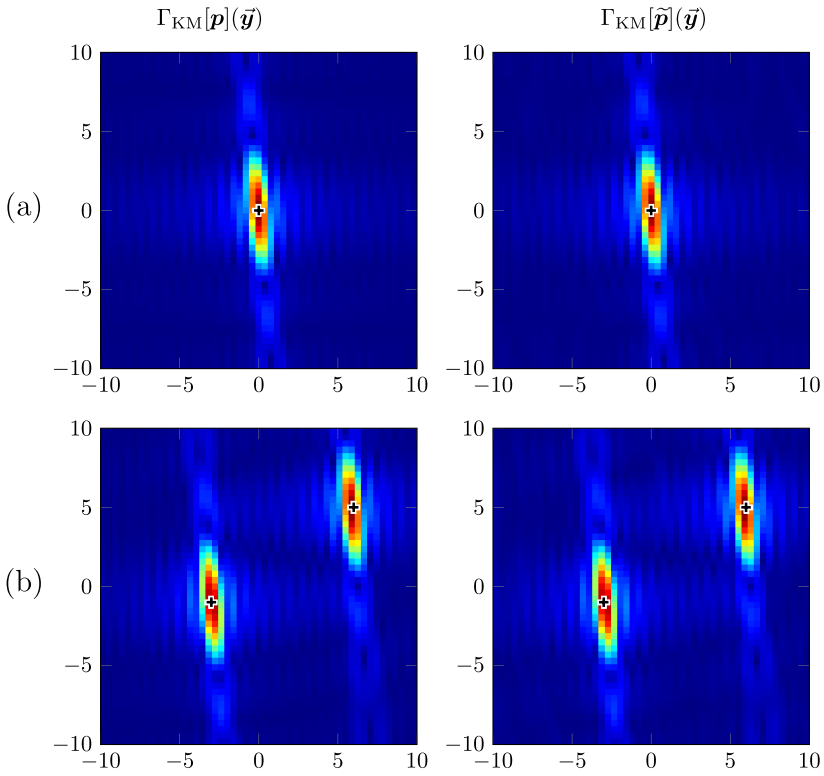

Figure 5. Kirchhoff images of (a) one and (b) two point scatterers whose true locations are indicated by crosses. The left column uses the full array response vector $\boldsymbol{p}$ while the right column uses the array response vector $\widetilde{\boldsymbol{p}}$ recovered from intensity data. The horizontal and vertical axes display the range and cross-range respectively, measured in central wavelengths λ_0 from (50, 0) mm.

frequency in figure 4(a) and the image using all the data in the bandwidth in figure 5(a). As predicted by our theoretical results, the images using the intensities are indistinguishable from the images using the data with phases. Although we are significantly undersampling on the array (recall the spacing between receivers is approx. 20 μm $\gg \lambda_0/2$), the images still exhibit the cross-range (Rayleigh) resolution estimate $\lambda_0 L/a \approx 5\lambda_0$. As expected the single frequency image has a poor range resolution (figure 4(a)). When all the frequencies in the bandwidth are used (figure 5(a)), the range resolution agrees with the well known estimate $c_0/|\mathcal{B}| \approx 1\lambda_0$, even with undersampling in the frequency band. Our second experiment (figure 4(b) for the single frequency image and figure 5(b) using the whole bandwidth) uses two point reflectors located at coordinates $\vec{\boldsymbol{y}}_1 = (50\,\mathrm{mm} - 3\lambda_0, -\lambda_0)$ and $\vec{\boldsymbol{y}}_2 = (50\,\mathrm{mm} + 6\lambda_0, 5\lambda_0)$ each with $\rho(\vec{\boldsymbol{y}}_i) = 1 \times 10^{-15}$. The images that are obtained appear to follow the same cross-range and range (only for the full bandwidth image) resolution estimates and are identical with or without phases. Finally, we show an extended scatterer (a disk) in figure 6. The disk is generated as a set of point reflectors, each with $\rho(\vec{\boldsymbol{y}}_i) = 1 \times 10^{-15}$ separated by $\lambda_0/4$.

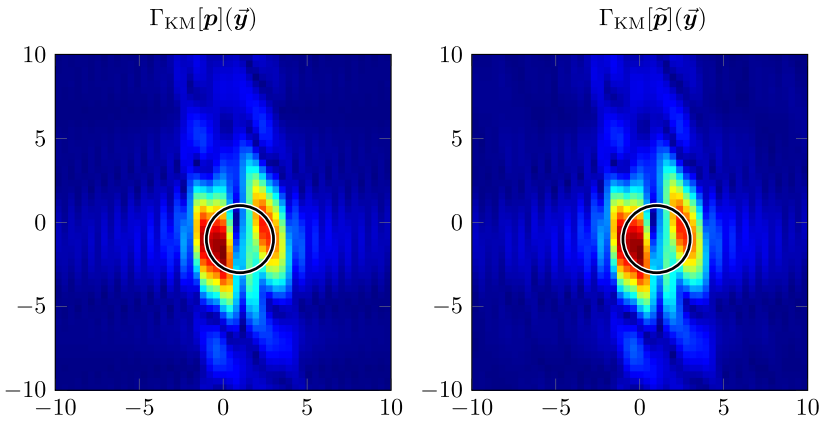

Figure 6. Kirchhoff images of an extended scatterer (disk). The boundary of the disk is indicated by the black and white circle. The left image uses the true array response vector $\boldsymbol{p}$ while the right image uses the array response vector $\widetilde{\boldsymbol{p}}$ recovered from intensity measurements. The horizontal and vertical axes display the range and cross-range respectively, measured in central wavelengths λ_0 from (50, 0) mm.

5.2. Stochastic illumination

Here we image with power spectrum data $\boldsymbol{d}$ generated from a stochastic illumination as in section 4. Since we work in an optic regime, adequately sampling signals in the time domain and performing the autocorrelations (19) is an expensive calculation. We instead use the Wiener–Khinchin theorem [20] to simulate power spectrum measurements directly.

We assume the wave source at $\vec{\boldsymbol{x}}_s$ is driven by a stationary mean zero Gaussian process $f(t)$ with correlation function $\langle \overline{f}(t) f(t+\tau)\rangle = F(\tau)$. By the Wiener–Khinchin theorem, $\widehat{f}(\omega)$ is a mean zero Gaussian process with correlation function

$$\langle \overline{\widehat{f}}(\omega)\widehat{f}(\omega')\rangle = 2\pi\delta(\omega-\omega')\widehat{F}(\omega). \tag{22}$$

Thus frequency samples of $\widehat{f}(\omega)$ are *independent* normal random variables with variance proportional to $\widehat{F}(\omega)$. Here we use

$$\widehat{F}(\omega) = t_{\mathrm{c}} \exp\left(\frac{-(\omega-\omega_0)^2}{4\pi/t_{\mathrm{c}}^2}\right), \tag{23}$$

where $(2\pi)^{-1}\omega_0 = 590$ THz is the central frequency and $t_{\mathrm{c}} = 150 \times 10^{-12}$ s is the correlation time of $f(t)$ (i.e. $F(\tau) \approx 0$ for $\tau \gg t_{\mathrm{c}}$). This choice of t_{c} gives the signal an effective frequency band of $(2\pi)^{-1}\mathcal{B} = [430, 750]$ THz (i.e. $\widehat{F}(\omega) \approx 0$ for $\omega \notin \mathcal{B}$). Using (22) and (23) we generate frequency samples $\widehat{f}(\omega_i)$ for 100 frequencies ω_i equally spaced in $\mathcal{B}$.

For a large enough acquisition time T, the empirical autocorrelations (19) give frequency domain measurements proportional to

$$\widehat{\psi}(\vec{\boldsymbol{x}}_r, \omega) = |\boldsymbol{e}_r^{\mathsf{T}}(\boldsymbol{g}_0 + \boldsymbol{p})\widehat{f}(\omega)|^2 \quad \text{for } r = 1,\ldots,N.$$

Thus for each frequency $\omega_i \in \mathcal{B}$ we generate the power spectrum data

$$\boldsymbol{d}(\vec{\boldsymbol{x}}_s, \omega_i) = \overline{((\boldsymbol{g}_0 + \boldsymbol{p})\widehat{f}(\omega_i))} \odot ((\boldsymbol{g}_0 + \boldsymbol{p})\widehat{f}(\omega_i)). \tag{24}$$

Because correlations are robust with respect to additive noise, we also consider autocorrelations with additive noise:

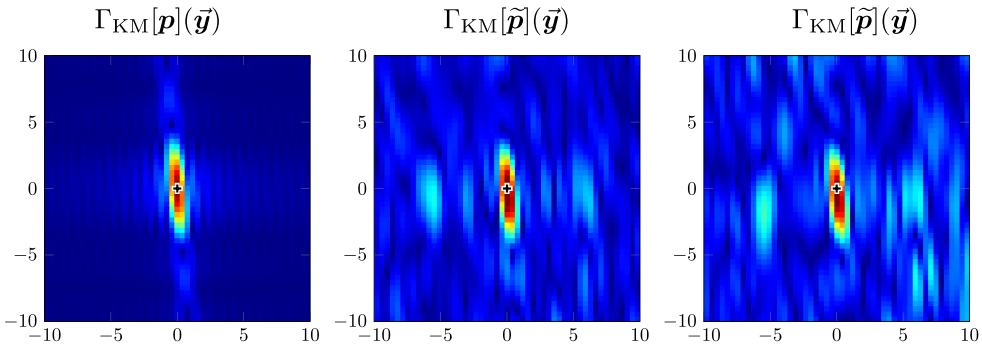

Figure 7. Kirchhoff images of a point scatterer using a stochastic illumination and autocorrelation measurements. The images are generated using (left) the true array response vector $\boldsymbol{p}$, (center) $\widetilde{\boldsymbol{p}}$ recovered from clean power spectrum data (24) and (right) $\widetilde{\boldsymbol{p}}$ recovered from noisy power spectrum data (25). The horizontal and vertical axes display the range and cross-range respectively, measured in central wavelengths λ_0 from (50, 0) mm.

$$\widehat{\psi}(\vec{\boldsymbol{x}}_r, \omega) = |\boldsymbol{e}_r^{\mathsf{T}}(\boldsymbol{g}_0 + \boldsymbol{p})\widehat{f}(\omega) + \widehat{\eta}_r(\omega)|^2 \quad \text{for } r = 1, \ldots, N,$$

where the noise $\widehat{\eta}_r(\omega)$ is an *independent* mean zero Gaussian process with correlation function given by (22) and (23) for each $r = 1, \ldots, N$. Here we set the noise power equal to 10% of the signal power at each receiver, i.e.

$$\int \mathrm{d}\omega\, |\widehat{\eta}_r(\omega)|^2 = \frac{1}{10} \int \mathrm{d}\omega\, |\boldsymbol{e}_r^{\mathsf{T}}(\boldsymbol{g}_0 + \boldsymbol{p})\widehat{f}(\omega)|^2, \quad \text{for } r = 1, \ldots, N.$$

Noisy data for each frequency $\omega_i \in \mathcal{B}$ is then generated as

$$\boldsymbol{d}(\vec{\boldsymbol{x}}_s, \omega_i) = \overline{((\boldsymbol{g}_0 + \boldsymbol{p})\widehat{f}(\omega_i) + \widehat{\boldsymbol{\eta}}(\omega_i))} \odot ((\boldsymbol{g}_0 + \boldsymbol{p})\widehat{f}(\omega_i) + \widehat{\boldsymbol{\eta}}(\omega_i)), \tag{25}$$

where $\widehat{\boldsymbol{\eta}}(\omega) = [\widehat{\eta}_1(\omega), \ldots, \widehat{\eta}_N(\omega)]^{\mathsf{T}}$. We can indeed consider noise with much larger power (e.g. noise power equal to 100% signal power), however to compensate we then need additional frequency samples to maintain sufficient averaging in migration images. In figure 7 we show the migrated images $\Gamma_{\mathrm{KM}}[\widetilde{\boldsymbol{p}}]$ for $\widetilde{\boldsymbol{p}} = (2\pi\widehat{F}\overline{\boldsymbol{g}}_0)^{-1} \odot \boldsymbol{d} - \boldsymbol{g}_0$ recovered from clean data (24) and from noisy data (25). We do not show single frequency images, as they are up to a scaling identical to the deterministic ones (figure 4).

5.3. Breakdown of the method

We now investigate situations where assumptions 1 and/or 2 are violated. For these experiments, we fix the receiver array $\mathcal{A}$ (again consisting of 501 receivers with locations $\vec{\boldsymbol{x}}_r$ given above) while varying the source position $\vec{\boldsymbol{x}}_s$, the reflector location $\vec{\boldsymbol{y}}$ and the reflectivity $\rho(\vec{\boldsymbol{y}})$. In figure 8 we show the migrated images of the recovered array response vector $\Gamma_{\mathrm{KM}}[\widetilde{\boldsymbol{p}}]$ for the following situations:

	Assumptions violated	$\vec{\boldsymbol{y}}$	$\rho(\vec{\boldsymbol{y}})$	$\vec{\boldsymbol{x}}_s$
(a) Source near scatterer	1 and 2	(50 mm, 0)	10^{-15}	(50 mm − $10\lambda_0$, 0)
(b) Receivers near scatterer	1	($11\lambda_0$, 0)	10^{-15}	(−50 mm, 0)
(c) Large reflectivity	1	(50 mm, 0)	10^{-10}	(5, −75) mm
(d) No geometric imaging condition	2	(50 mm, 0)	10^{-15}	(5 mm, 0)

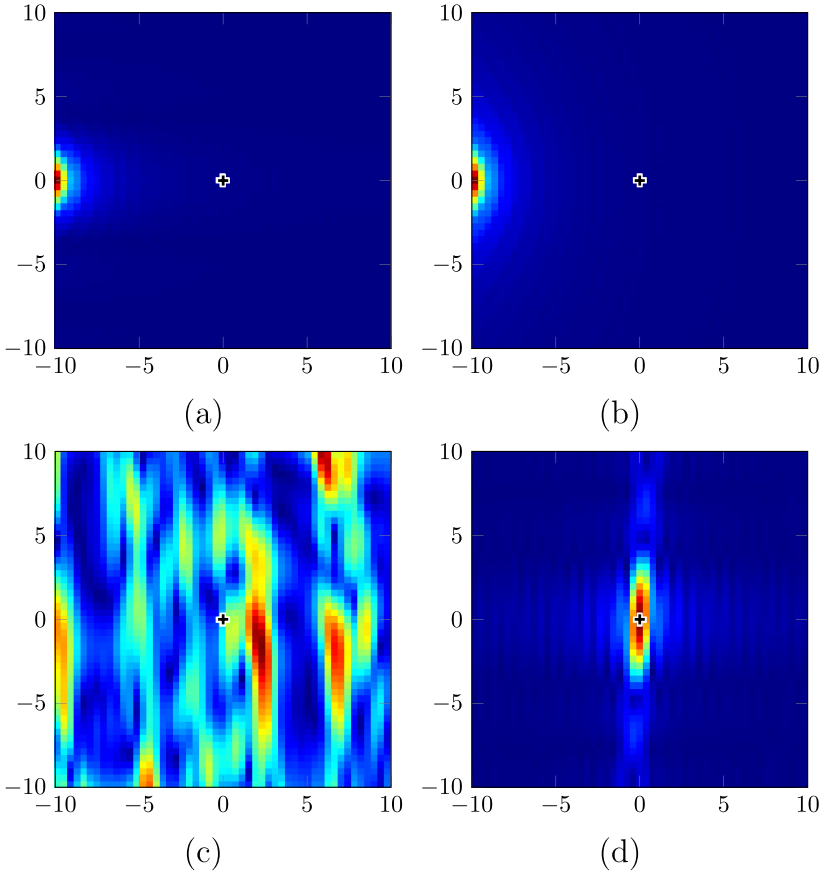

Figure 8. Breakdown of imaging method: migrated images $\Gamma_{\mathrm{KM}}[\widetilde{\boldsymbol{p}}]$ for setups violating assumptions 1 and/or 2. Details of each setup are listed above and correspond to (a) $\vec{\boldsymbol{x}}_s$ placed to close to $\vec{\boldsymbol{y}}$, (b) $\mathcal{A}$ placed too close to $\vec{\boldsymbol{y}}$, (c) large reflectivity ρ and (d) $\vec{\boldsymbol{x}}_s$ placed in front of the array $\mathcal{A}$. The axes are measured in central wavelengths λ_0 from the scatterer's true location $\vec{\boldsymbol{y}}$ which is indicated by a cross.

From figures 8(a)–(c) we see the imaging method is most sensitive to breaking assumption 1. In these situations the quadratic term $\overline{\boldsymbol{p}} \odot \boldsymbol{p}$ cannot be neglected in the intensity data (8) and thus the linear system we consider in (9) is no longer a good approximation. This leads to artifacts in the images. Figure 8(d) demonstrates the imaging method is more robust than expected with respect to assumption 2 and the position of $\vec{\boldsymbol{x}}_s$.

6. Discussion and future work

We have shown that when the scattered field is small compared to the incident field (assumption 1), one can consider the problem of recovering full-waveform data from intensity measurements as a linear least-squares problem. For N receivers, the corresponding real matrix is $N \times 2N$ so all we can expect to recover is the projection of the real and imaginary

parts of the full-waveform data onto an N-dimensional subspace. This turns out to be sufficient to image with Kirchhoff migration (theorem 1). Crucially we do not need to manipulate the fields at the receiver end, e.g. to introduce phases. The least-squares problems we obtain are usually well-conditioned and the computational cost of solving them ($\mathcal{O}(N)$ complex operations, each) is negligible compared to the cost of Kirchhoff migration. Since we make no assumptions on the source phases, our method adapts well to situations where the source is driven by a Gaussian process and the measurements are autocorrelations at the receiver locations.

The fundamental principle we have used here is that the imaging method (in this case Kirchhoff migration) does not require all the data (in this case the full-waveform scattered field) to form an image. For Kirchhoff migration this is exploited e.g. by undersampling in frequency and/or using only a few sources or receivers to image. We have shown that there is another way in which one can use incomplete data, as projections of the array response vector on certain subspaces leave the Kirchhoff images unaffected. A similar principle is what is exploited by Novikov *et al* [25] to image with intensities, since they show that knowing inner products of single source experiments is enough to image with MUSIC. It would be interesting to carry this idea further and see whether the same preprocessing we use here works for MUSIC and also whether it is possible to image scatterers with even less data.

Acknowledgments

The work of P Bardsley and F Guevara Vasquez was partially supported by the National Science Foundation grant DMS-1411577.

References

[1] Balan R, Casazza P and Edidin D 2006 On signal reconstruction without phase *Appl. Comput. Harmon. Anal.* **20** 345–56
[2] Bardsley P and Guevara Vasquez F 2016 Imaging with power controlled source pairs *SIAM J. Imaging Sci.* **9** 185–211
[3] Bleistein N and Handelsman R A 1986 *Asymptotic Expansions of Integrals* 2nd edn (New York: Dover)
[4] Bleistein N, Cohen J K and Stockwell J W Jr 2001 *Mathematics of Multidimensional Seismic Imaging, Migration, and Inversion* (*Interdisciplinary Applied Mathematics* vol 13) (New York: Springer)
[5] Candès E J, Strohmer T and Voroninski V 2013 PhaseLift: exact and stable signal recovery from magnitude measurements via convex programming *Commun. Pure Appl. Math.* **66** 1241–74
[6] Casazza P G and Woodland L M 2014 Phase retrieval by vectors and projections *Operator Methods in Wavelets, Tilings, and Frames* (*Contemporary Mathematics* vol 626) (Providence, RI: American Mathematical Society) pp 1–7
[7] Chai A, Moscoso M and Papanicolaou G 2011 Array imaging using intensity-only measurements *Inverse Problems* **27** 015005
[8] Chen Z and Huang G 2015 Phaseless imaging by reverse time migration: acoustic waves arXiv:1502.00957
[9] Cheney M 2001 The linear sampling method and the MUSIC algorithm *Inverse Problems* **17** 591–5
[10] Crocco L, D'Urso M and Isernia T 2004 Inverse scattering from phaseless measurements of the total field on a closed curve *J. Opt. Soc. Am.* A **21** 622–31
[11] Devaney A J 1989 Structure determination from intensity measurements in scattering experiments *Phys. Rev. Lett.* **62** 2385–8
[12] Fienup J R 1982 Phase retrieval algorithms: a comparison *Appl. Opt.* **21** 2758–69

[13] Garnier J and Papanicolaou G 2009 Passive sensor imaging using cross correlations of noisy signals in a scattering medium *SIAM J. Imaging Sci* **2** 396–437
[14] Garnier J and Papanicolaou G 2010 Resolution analysis for imaging with noise *Inverse Problems* **26** 074001
[15] Garnier J, Papanicolaou G, Semin A and Tsogka C 2015 Signal to noise ratio analysis in virtual source array imaging *SIAM J. Imaging Sci.* **8** 248–79
[16] Gbur G and Wolf E 2002 Diffraction tomography without phase information *Opt. Lett.* **27** 1890–2
[17] Gbur G and Wolf E 2004 The information content of the scattered intensity in diffraction tomography *Inform. Sci.* **162** 3–20
[18] Gerchberg R and Saxton W 1972 A practical algorithm for the determination of phase from image and diffraction plane pictures *Optik* **35** 237–46
[19] Holmes R B and Belen'kii M S 2004 Investigation of the Cauchy–Riemann equations for one-dimensional image recovery in intensity interferometry *J. Opt. Soc. Am.* A **21** 697–706
[20] Ishimaru A 1997 *Wave Propagation and Scattering in Random Media* (*IEEE/OUP Series on Electromagnetic Wave Theory*) (New York: IEEE)
[21] Klibanov M V 2014 Uniqueness of two phaseless non-overdetermined inverse acoustics problems in 3d *Appl. Anal.* **93** 1135–49
[22] Klibanov M V and Sacks P E 1992 Phaseless inverse scattering and the phase problem in optics *J. Math. Phys.* **33** 3813–21
[23] Klibanov M V and Sacks P E 1994 Use of partial knowledge of the potential in the phase problem of inverse scattering *J. Comput. Phys.* **112** 273–81
[24] Maleki M H and Devaney A J 1993 Phase-retrieval and intensity-only reconstruction algorithms for optical diffraction tomography *J. Opt. Soc. Am.* A **10** 1086–92
[25] Novikov A, Moscoso M and Papanicolaou G 2014 Illumination strategies for intensity-only imaging *SIAM J. Imaging Sci.* **8** 1547–73
[26] Olver F W J, Lozier D W, Boisvert R F and Clark C W (ed) 2010 *NIST Handbook of Mathematical Functions* (New York: Cambridge University Press)
[27] Schmitt J 1999 Optical coherence tomography (OCT): a review *IEEE J. Sel. Top. Quantum Electron.* **5** 1205–15
[28] Schmitt J, Lee S and Yung K 1997 An optical coherence microscope with enhanced resolving power in thick tissue *Opt. Commun.* **142** 203–7
[29] Schuster G T 1996 Resolution limits for crosswell migration and traveltime tomography *Geophys. J. Int.* **127** 427–40
[30] Schuster G T 2009 *Seismic Interferometry* (Cambridge: Cambridge University Press)
[31] Schuster G T, Yu J, Sheng J and Rickett J 2004 Interferometric/daylight seismic imaging *Geophys. J. Int.* **157** 838–52
[32] Takenaka T, Wall D J N, Harada H and Tanaka M 1997 Reconstruction algorithm of the refractive index of a cylindrical object from the intensity measurements of the total field *Microw. Opt. Technol. Lett.* **14** 182–8
[33] Teague M R 1983 Deterministic phase retrieval: a Green's function solution *J. Opt. Soc. Am.* **73** 1434–41
[34] Yin P and Xin J 2015 PhaseLiftOff: an accurate and stable phase retrieval method based on difference of trace and Frobenius norms *Commun. Math. Sci.* **13** 1033–49